

A continuous constraint satisfaction problem for the rigidity transition in confluent tissues

Pierfrancesco Urbani¹

¹Université Paris-Saclay, CNRS, CEA, Institut de physique théorique, 91191, Gif-sur-Yvette, France

Models of confluent tissues are built out of tessellations of the space (both in two and three dimensions) in which the cost function is constructed in such a way that individual cells try to optimize their volume and surface in order to reach a target shape. At zero temperature, many of these models exhibit a rigidity transition that separates two phases: a liquid phase and a solid (glassy) phase. This phenomenology is now well established but the theoretical understanding is still not complete.

In this work we introduce an exactly soluble mean field model for the rigidity transition which is based on an abstract mapping. We replace volume and surface functions by random non-linear functions of a large number of degrees of freedom forced to be on a compact phase space. We then seek for a configuration of the degrees of freedom such that these random non-linear functions all attain the same value. This target value is a control parameter and plays the role of the target cell shape in biological tissue models. Therefore we map the microscopic models of cells to a random continuous constraint satisfaction problem (CCSP) with *equality* constraints. We show that at zero temperature, the rigidity transition corresponds to the satisfiability transition of the problem. We also characterize both the satisfiable (SAT) and unsatisfiable (UNSAT) phase. In the SAT phase we show that before reaching the rigidity transition, the zero temperature SAT landscape undergoes an RSB/ergodicity breaking transition of the same type as the Gardner transition in amorphous solids. In the UNSAT phase we compute the average shape index as a function of the target one and we compare the thermodynamical solution of the model with the results of the numerical minimization of the corresponding cost function.

I. INTRODUCTION

In recent years there has been a growing interest in understanding the properties of biological tissues. Tissues can be in different phases: liquid tissues like the blood can (and do) coexist with solid tissues like the epithelial one. Often, among the same tissue one can see both liquid and solid phases. This is for example the case of tumors inside healthy solid tissues which are often found to have a core-periphery structure [1, 2] in which the core has solid-like (or subdiffusive) nature while the periphery is more liquid-like (or superdiffusive). This is crucial to understand metastasis formation and their migration in the organism.

Of course the microscopic organization of cells inside individual tissues, changes a lot depending on the nature of the tissue. The gray and white matter in the brain share very little with how cells are organized in the skin. In the former, the structure of long, up to brain-size, axons and dendrites [3] share more similarities with polymer networks. This structure has been thought to play a role in the gyration mechanisms both in the cerebral and cerebellar cortex [4, 5]. Packing of compact objects, like colloidal glasses are instead qualitatively closer to epithelial tissues. Among different types of tissues, confluent ones have very simple structure. Inside the skin, cells tassellate the space in a rather uniform (yet non-crystalline) manner forming an elastic sheet.

Recently the problem of characterizing the properties of confluent tissues has attracted a lot of interest in the context of active matter [6, 7]. Indeed cells can self-propel and migrate and therefore including the effect of this self propulsion may be important to understand their macroscopic behavior.

Simple models of confluent tissues are Vertex [8] or Voronoi models [6]. In both of them, the degrees of freedom realize a convex tessellation of the space[39] (both in two and three dimensions). Given a tessellation, its cost is defined as a sum of surface and volume terms: each cell in the tessellation tries to attain a target volume (area in $2d$) and surface (perimeter in $2d$). The target volume and surface are not completely independent control parameter: given a target volume it is clear that the target surface cannot be smaller than the one of the sphere (or disk in $2d$) having that target volume. Conversely, a single cell can have a very small volume while having large surface (think about a thin parallelepiped with one dimension much smaller than the other two). However cells need to tassellate the space and therefore fluctuations to anomalously small volumes are unlikely due to the confluence constraint.

In order to characterize the behavior of these systems, one can define a target shape index as the adimensional combination of the target surface and volume. Recently it has been found that driving the target shape index, one can induce a rigidity transition in these models. The transition splits the phase diagram into two regions: a liquid phase where cells can diffuse in space, and a solid phase where cells are trapped into an amorphous configuration. Both solids and liquid phases can survive when some driving is switched on (both thermal or active).

In order to characterize the transition, a series of studies have focused on the landscape of these models at zero temperature [9–11]. In the zero temperature liquid phase, the degrees of freedom manage to find a configuration in which each cell attains the target volume and surface. Instead in the solid phase cells do not manage to achieve their target shape and are stuck in a local minimum of the corresponding energy landscape.

In this work we develop a simple mean field model for the rigidity transition in confluent tissues. In order to do that we take an abstraction step: seen from a purely optimization point of view, one can think about volume and surface constraints as non-linear *equality* constraints. The minimization of the energy function in tissue models corresponds to finding a configuration of the degrees of freedom such that volume and surface functions are equal to some control parameter. Therefore we replace volume and surface functions by non-linear functions. Since the landscape in tissue models is glassy, we will consider random non-linear functions which automatically generate a complex energy landscape. Therefore we map the zero temperature minimization problem to a random constraint satisfaction problem with continuous variables (CCSP) and *equality* constraints. We will analyze the problem through the replica method and investigate the properties of the SAT and UNSAT landscape and of the zero temperature transition as well.

The manuscript is organized as follows. First we describe the models of two and three dimensional confluent tissues, we review their behavior and map them to random CCSP with equality constraints. Then we solve the CCSP and characterize the liquid (SAT) phase and solid (UNSAT) phase.

II. A CCSP FOR THE RIGIDITY TRANSITION OF CONFLUENT TISSUES

A. Models of confluent tissues

Simple models of confluent tissues are Vertex and Voronoi models. To fix the ideas we will focus on two dimensions but everything can be generalized to higher dimensions. In vertex models one has a network of vertices connected by non-intersecting links of varying length. These links define a tessellation of space. The degrees of freedom are the position of the vertices. In Voronoi models instead, one has a fixed number of points, the centers of the cells and construct the Voronoi tessellation out of them. For both models the energy function is given in terms of the cells that form the tessellation of the space. Denoting by A_i and P_i the corresponding area and perimeter of the cell i , the Hamiltonian of the system is written as

$$H[\underline{x}] = \frac{1}{2} \sum_{i=1}^M [k_A(A_i(\underline{x}) - A_0)^2 + k_P(P_i(\underline{x}) - P_0)^2] \quad (1)$$

where we have denoted by \underline{x} the collective position in phase space of the degrees of freedom and k_A and k_P are elastic constants. We assume that the dimension of the vector \underline{x} is N which is the system size [40]. Instead M is the number of cells. The Euler characteristic formula then connects M , N and the number of links defining the perimeters of the cells with the genus of the surface that is tessellated.

In the zero temperature limit one can attain a zero energy $H = 0$ if all areas and perimeters match their target values. For the Voronoi model this is not possible in general because $M = N/2$ and therefore one has a number of constraints that is equal to the number of degrees of freedom [9] (note that in 2d the number of degrees of freedom is $N = 2M$). In three dimensions instead the number of degrees of freedom is $N = 3M$ which is larger than the number of constraints coming from volume and surface and therefore one can have a genuine liquid phase, where $H = 0$ [10, 12]. Note that removing the area term in Eq. (1) gives rise to a well defined model which can undergo a rigidity transition [13]. Vertex models instead are typically underconstrained since the number of degrees of freedom are typically larger than the number of cells [6]. A detailed counting of degrees of freedom and constraints can be found in [11, 12]. In order to induce a rigidity transition one typically consider the setting in which $A_0 = A_{TOT}/M$, namely the cells tessellate the space (being A_{TOT} the total area of the system) and change P_0 . For large values of P_0 , underconstrained models (namely models for which the number of degrees of freedom is larger than the number of constraints) exhibit a liquid phase ($H = 0$). In particular by running some greedy descent on Eq. (1) it is possible to find a zero energy configuration with an extensive number of zero modes (whose number scales as the number of degrees of freedom subtracted by total number of constraints). Decreasing P_0 one can cross a rigidity transition where greedy search algorithms do not manage to find zero energy configurations. The density of states in this case does not have zero modes [13].

In order to characterize the critical point one can define the target shape index, a dimensionless control parameter defined as $s_0 = P_0/\sqrt{A_0}$. Furthermore one can also define the average shape index as $s = \langle P \rangle / \sqrt{\langle A \rangle}$ where $\langle P \rangle = \sum_{i=1}^M P_i$ and $\langle A \rangle = \sum_{i=1}^M A_i$ are the average perimeter and area respectively. In the liquid phase, at zero temperature,

$s_0 = s$. Reducing s_0 , one can cross the critical point at s_0^* . Below this point s varies very weakly and stays roughly close to s_0^* [10]. The value of s_0^* depends on the geometry of the problem and on the dimension [8–10].

B. The mapping to random CCSPs with equality constraints

In order to make a simple mean field model for these systems, we follow the same route that has been recently developed to study the jamming transition in spheres and non-spherical particles [14–20]. In these cases the constraints of non-overlapping particles is replaced by a set of random excluded volume constraints for a set of continuous variables. In the end one gets a CCSP with *inequality* constraints. The corresponding models are very effective in describing the physics of 2d and 3d systems. It is very remarkable the case of jamming of spherical particles where the critical exponents of the transition in the infinite dimensional treatment [21, 22] are the very same as the one the random CCSP models [15, 18] and agree within numerical precision with numerical simulations in 2d and 3d systems[23, 24]. For non-spherical particles the models reproduce all features of the jamming/rigidity transition in particular the complex structure of the density of states [16, 17].

In order to define a simple mean field model for the rigidity transition in confluent tissues, we start by considering an N -dimensional vector $\underline{x} = \{x_1, \dots, x_N\}$ subjected to a spherical constraint $|\underline{x}|^2 = N$ which defines a compact phase space. From an optimization point of view the Hamiltonian in Eq. (1) is a square loss function. We replace the functions $A_i(\underline{x})$ and $P_i(\underline{x})$ by a set of non-linear functions $h_\mu(\underline{x})$. The Hamiltonian of the model is

$$H[\underline{x}] = \frac{1}{2} \sum_{\mu=1}^M (h_\mu(\underline{x}) - p_0)^2. \quad (2)$$

Note that the constraint counting is not the same as in Eq. (1) since there is no distinction between area and perimeter. However this is not very important since what matters is how the number of constraints M compares with the number of degrees of freedom N . If the reader wants to have in mind a direct mapping, one can consider the Voronoi model in 2d with $k_A = 0$. In this case $M = N/2$. On general grounds we will choose $M < N$ and in particular we will scale $M = \alpha N$ with $\alpha < 1$.

We choose the functions $h_\mu(\underline{x})$ to be random non-linear functions. The simplest example is

$$h_\mu(\underline{x}) = \frac{1}{N} \sum_{i < j} J_{ij}^\mu x_i x_j. \quad (3)$$

The components of the $M = \alpha N$ random matrices J_{ij}^μ , with $\mu = 1, \dots, M$ and $i, j = 1, \dots, N$ are i.i.d. random Gaussian variables with zero mean and unit variance. We assume that the matrix is symmetric under index permutations. Note that the scaling with the system size N is such that $h_\mu(\underline{x})$ is a random quantity of order one. The control parameter p_0 in Eq. (2) plays the same role as the target perimeter in the Voronoi model in 2d and therefore we will refer to it as the target shape index.

On a purely qualitative level, the model defined in Eq. (2) is of the same form as the one in Eq. (1). We are interested in studying the landscape of this model at zero temperature (and then, possibly, increasing the temperature). The control parameters, at zero temperature are α and p_0 .

The intuitive physics of the model can be summarized as follows. For $\alpha < 1$ and sufficiently small p_0 , there exist, with high probability, configurations \underline{x} that are at zero energy and therefore such that $h_\mu(\underline{x}) = p_0$ for all $\mu = 1, \dots, \alpha N$. This is because, for random \underline{x} the variables h_μ are Gaussian numbers with zero mean and therefore we expect that it is easy to find a configuration with h_μ nearly zero. In other words a random \underline{x} is close to be a solution of the CCSP for $p_0 \sim 0$. We say that for small values of p_0 the model exhibits a zero temperature liquid phase which is satisfiable (SAT). Conversely increasing p_0 one is forced to sample the tail of the Gaussian distribution up to the point that finding a zero energy configuration becomes a large deviation. This point is the SAT/UNSAT transition. At large enough p_0 the model is in the unsatisfiable (UNSAT) phase and minimizing the Hamiltonian one ends up in a local minimum.

Note that, with respect to confluent tissues where the transition from liquid to solid is crossed *decreasing* p_0 , here we need to *increase* it (or decrease it to negative values). However this difference is immaterial and depends only on the geometry of the problem.

In the following we will solve the thermodynamics of the model at zero temperature. We underline that a dynamical treatment of the model through dynamical mean field theory is possible and will be developed in a forthcoming work. It will allow to include in the analysis the effect of non-conservative forces (shear drive or activity) and to discuss its differences with thermal noise (whose effect can be instead described by the formalism here below).

1. Generalization of the model

Before discussing the full solution of the model, we mention how it can be generalized to generic non-linear functions $h_\mu(\underline{x})$. Indeed one can generically define $h_\mu(\underline{x})$ to be random Gaussian functions with correlations defined by

$$\overline{h_\mu(\underline{x})h_\mu(\underline{y})} = g\left(\frac{\underline{x} \cdot \underline{y}}{N}\right) \quad (4)$$

where we have denoted by the \cdot the Euclidean scalar product between two vectors and by the overline the average over the realization of these functions. The special case considered in Eq. (3) corresponds to $g(q) = q^2/2$. A way to realize the covariances in Eq. (4) is to consider the following form for $h_\mu(\underline{x})$

$$h_\mu(\underline{x}) = \sum_{\tau=1}^{\infty} a_\tau N^{-\tau/2} \sum_{i_1 < \dots < i_\tau} J_{i_1 i_2 \dots i_\tau}^\mu x_{i_1} x_{i_2} \dots x_{i_\tau} \quad (5)$$

where $J_{i_1 i_2 \dots i_\tau}^\mu$ are rank τ tensors with Gaussian components with zero mean and unit variance and a_τ are constants. Then, the function g acquires the following Taylor expansion form

$$g(q) = a_1^2 q + a_2^2 \frac{q^2}{2} + \dots a_\tau^2 \frac{q^\tau}{\tau!} + \dots \quad (6)$$

A model of a similar kind of Eq. (2) with general covariances as in Eq. (4) was considered in [25] as a model for non-linear encryption of a high dimensional signal. However, crucially, in [25] only the $\alpha > 1$ case was analyzed (this is the regime where signal reconstruction can be information theoretically possible). Furthermore, in [25] p_0 depends itself on the index μ and it is correlated with an underlying signal, while here we consider it to be fixed and use it as a control parameter. Both ingredients ($\alpha < 1$ and p_0 constant) are essential to obtain a model having a rigidity transition at zero temperature.

III. SOLUTION OF THE MODEL

A. The replica approach

We are interested in studying whether the model has a rigidity transition as a function of p_0 . In order to compute the phase diagram we start by looking at the partition function at inverse temperature $\beta = 1/T$. We will be interested in the limit $T \rightarrow \infty$ and look for the properties of the ground states. The partition function is defined as

$$Z = \int_{|\underline{x}|^2 = N} d\underline{x} e^{-\beta H[\underline{x}]} \quad (7)$$

and we are interested in looking at the average free entropy which is given by

$$f = \frac{1}{N\beta} \overline{\ln Z} . \quad (8)$$

Again, the overline stands for the average over the random couplings which provide a realization of the non-linear functions h_μ . In the SAT phase, at zero temperature, f gives the entropy of zero energy configurations. Conversely, in the UNSAT phase, f is nothing but minus the ground state energy.

The average over the disorder in Eq. (8) can be carried on using the replica method. Indeed the average free entropy can be written in terms of the replicated partition function through the famous formula [26]

$$f = \frac{1}{\beta N} \lim_{n \rightarrow 0} \overline{Z^n} . \quad (9)$$

For integer value of n one can write $\overline{Z^n}$ as

$$\overline{Z^n} = \int dQ e^{nS[Q]} \quad (10)$$

where the action $S[Q]$ is given by

$$S[Q] = \frac{1}{2} \ln \det Q + \alpha \ln \mathcal{Z} . \quad (11)$$

The partition function \mathcal{Z} of the 'impurity' problem is given by

$$\mathcal{Z} = \exp \left[\frac{1}{2} \sum_{ab=1}^n g(Q_{ab}) \frac{\partial^2}{\partial h_a \partial h_b} \right] \prod_{a=1}^n e^{-\frac{\beta}{2}(h_a - p_0)^2} \Big|_{h=0} . \quad (12)$$

This quantity gives the local partition function corresponding to a random function h which is in the bath of all the others (from which the name of 'impurity' problem).

The derivation of these formulas follows straightforwardly standard manipulations, see [15] for a detailed reference on a very similar computation. Note that the impurity problem can be solved exactly due to the fact that it can be transformed into a Gaussian integral which can be treated through standard techniques in replica theory, see the appendix of [27]. However we prefer to stay within the present formalism since it will be convenient for future computations. In the large N limit, the order parameter is the overlap matrix Q_{ab} which is determined by a saddle point condition. At saddle point we can interpret it as $Q_{ab} = \langle \mathbf{x}_a \cdot \mathbf{x}_b \rangle / N$ which is the overlap between two replicas extracted with the Boltzmann measure. Following [26], the matrix Q can be parametrized, in the most general replica symmetry breaking (RSB) form, by a function $x(q) : [0 < q_m, q_M < 1] \rightarrow [0, 1]$ which encodes for the cumulative distribution of the overlap between two replicas extracted from the corresponding Boltzmann measure. The saddle point for the function $x(q)$ can be written in the following way. We have a first non-linear partial differential equation (PDE) [28]

$$\begin{cases} \frac{\partial m(q, h)}{\partial q} = -\frac{1}{2} \frac{\partial g(q)}{\partial q} \left[\frac{\partial^2 m(q, h)}{\partial h^2} + 2x(q)m(q, h) \frac{\partial m(q, h)}{\partial h} \right] \\ m(q_M, h) = \frac{\partial}{\partial h} \ln \int_{-\infty}^{\infty} \frac{1}{\sqrt{2\pi(g(1) - g(q_M))}} e^{-z^2/(2(g(1) - g(q_M))) - \frac{1}{2}\beta(h - z)^2} \end{cases} \quad (13)$$

which should be solved at fixed $x(q)$. In order to shorten the notation, we indicate with a prime the derivative w.r.t. h and with a dot the derivatives w.r.t. q . Together with Eq. (13), one has a linear PDE given by [29]

$$\begin{cases} \frac{\partial P(q, h)}{\partial q} = \frac{\dot{g}(q)}{2} [P''(q, h) - 2x(q)(P(q, h)m(q, h))'] \\ P(q_m, h) = \frac{\exp[-(h+p_0)^2/(2g(q_m))]}{\sqrt{2\pi g(q_m)}} \end{cases} \quad (14)$$

Finally we have an equation for $x(q)$ in terms of the solution of the PDEs above. This equation is written as

$$\frac{q_m}{\lambda^2(q)} + \int_{q_m}^q \frac{dp}{\lambda^2(p)} = \alpha \dot{g}(q) \int_{-\infty}^{\infty} dh P(q, h) m^2(q, h) \quad (15)$$

From the solution of Eq.(13),(14) and (15) we can find the profile of $x(q)$. It is useful to take two derivatives w.r.t. q of Eq.(15). The first derivative gives the following equation

$$\frac{1}{\lambda^2(q)} = \alpha \int_{-\infty}^{\infty} dh P(q, h) [\ddot{g}(q)m^2(q, h) + (\dot{g}(q))^2 (m'(q, h))^2] . \quad (16)$$

The second derivative instead gives

$$x(q) = \frac{\lambda(q)}{2} \frac{\alpha \int_{-\infty}^{\infty} dh P(q, h) [\ddot{g}(q)m^2(q, h) + 4\alpha \dot{g}(q)\ddot{g}(q)(m'(q, h))^2 + (\dot{g}(q))^3 (m''(q, h))^2]}{\lambda^{-2}(q) + \alpha \lambda(q) (\dot{g}(q))^3 \int_{-\infty}^{\infty} dh P(q, h) (m'(q, h))^3} . \quad (17)$$

In both equations we have defined $\lambda(q)$ as

$$\lambda(q) = 1 - q_M + \int_q^{q_M} dp x(p) . \quad (18)$$

We will study the solution of these equations in detail both in the SAT phase and in the UNSAT phase. It is useful to derive the equation for the average value of h_μ . Following the same strategy used in [15] we get

$$\bar{h} = \overline{\frac{1}{M} \sum_{\mu=1}^M h_\mu} = p_0 - \frac{1}{\beta} \int_{-\infty}^{\infty} dh P(q_M, h) m(q_M, h) \quad (19)$$

This can be interpreted as the average shape index and should be compared with the target one p_0 . At zero temperature, in the SAT phase, we expect $p_0 = \bar{h}$ while in the UNSAT phase this will not be true anymore.

Note that for the moment, all the equations we wrote work for any temperature. Before focusing on the solution of these equations we will focus on a simpler case that gives rise to a convex optimization/constraint satisfaction problem and that can be solved fully analytically.

B. A simple case: the convex problem

We will consider the case in which $g(q) = q$. This case corresponds to

$$h_\mu(\underline{x}) = \frac{\xi^\mu \cdot \underline{x}}{\sqrt{N}} \quad (20)$$

with $\xi^\mu = \{\xi_1^\mu, \dots, \xi_N^\mu\}$ a random vectors with Gaussian entries with zero mean and unit variance. In this case, the SAT phase corresponds to solve an underconstrained linear system of equations. However, since the vector \underline{x} is constrained to be on the hypersphere $|\underline{x}|^2 = N$, a solution to the linear system will exist only up to a critical value p_0 . The Hamiltonian is however convex in the degrees of freedom and therefore the landscape of the problem is simple: in the SAT phase it corresponds to a single ergodic region at zero energy while in the UNSAT phase it is made by a single minimum. This means that the problem is replica symmetric which implies that $q_m = q_M = q$ and there is no $x(q)$ to take into account for. The saddle point equation for q in the zero temperature SAT phase is

$$\frac{q}{(1-q)^2} = \alpha \frac{q + p_0^2}{(1-q)^2}. \quad (21)$$

At the SAT/UNSAT transition point we expect that $q \rightarrow 1$ since the space of solutions reduces to a single point. Therefore the critical point is given by

$$p_0^* = \left(\frac{1}{\alpha} - 1 \right)^{\frac{1}{2}} \quad (22)$$

Note that the RS solution is stable against RSB as can be checked by a de Almeida-Thouless [30] stability analysis which in this case gives that the solution is stable for $\alpha \leq 1$. Note that $\alpha = 1$ corresponds also to an upper bound for the SAT phase in a system of random linear equations. It is also useful to compute the average shape index \bar{h} . This is trivially equal to p_0 in the SAT phase as can be checked by inspection using Eq. (19). In the UNSAT phase instead one needs to compute the solution of the RS equations. In this case, since the system sits in a minimum of the energy landscape, we expect that $q = 1 - \chi T$ being $T \rightarrow 0$ the temperature. The saddle point equation for χ is given by

$$\frac{1}{\chi^2} = \alpha \frac{1 + p_0^2}{(1 + \chi)^2} \quad (23)$$

and we note that the unjamming transition corresponds to the limit in which $\chi \rightarrow \infty$ since this solution needs to match with the one in the SAT phase where $q < 1$. This limit gives the correct SAT/UNSAT transition point as in Eq. (22). Equipped with the equation for the order parameter χ in the UNSAT phase, we can look at the average shape index. This is given by

$$\bar{h} = \begin{cases} p_0 & p_0 \leq p_0^* \\ \frac{p_0 \chi}{1 + \chi} = \left(\frac{p_0^2}{\alpha(1 + p_0^2)} \right)^{\frac{1}{2}} & p_0 > p_0^*. \end{cases} \quad (24)$$

In the limit in which $p_0 \rightarrow \infty$ the average shape index goes to a constant $\bar{h} \rightarrow \alpha^{-\frac{1}{2}}$.

C. The SAT/liquid phase

We will now consider the more generic setting in which $g(q)$ is non-linear giving rise a non-convex optimization/constraint satisfaction problem. To fix the ideas we will derive the results for the case $g(q) = q^2/2$ which is the simplest one (also for numerical simulations). We note that in this case, the Hamiltonian is invariant under spin inversion symmetry meaning that Eq. (3) is unchanged under $x_i \rightarrow -x_i$. The generic replica symmetric equation for $q_m = q_M = q < 1$ is

$$\frac{q}{(1-q)^2} = \alpha \dot{g}(q) \frac{g(q) + p_0^2}{(g(1) - g(q))^2}. \quad (25)$$

For $g(q) = q^2/2$ we get

$$\frac{q}{(1-q)^2} = 2\alpha q \frac{q^2 + 2p_0^2}{(1-q^2)^2}. \quad (26)$$

This equation admits a solution $q = 0$ which indeed respects spin inversion symmetry. The stability of the replica symmetric solution is controlled by the de Almeida-Thouless condition which reads

$$\frac{q}{(1-q)^2} = \alpha \dot{g}(q) \frac{1}{(g(1) - g(q))^2} + \alpha \ddot{g}(q) \frac{g(q) + p_0^2}{(g(1) - g(q))^2}. \quad (27)$$

For the $g(q) = q^2/2$, using the RS solution $q = 0$ we get

$$1 = 4\alpha p_0^2 \quad (28)$$

which implies that the RS solution is stable up for $p_0 < p_0^G$ being the RSB transition point given by

$$p_0^G = 2\alpha^{-1/2}. \quad (29)$$

At the transition point we can compute the breakpoint of the RSB solution [26] from Eq. (17) to get that $x = 0$. This implies that the RSB transition is continuous. Whether the ergodicity broken phase is of fullRSB type or finite RSB type must be checked by computing the 'slope' of the overlap profile $q(x)$ (the inverse function of $x(q)$). However the formalism we have written includes the case of finite RSB solutions and since we are going to explicitly solve the equations we will not pursue into this Landau analysis close to the critical point [31].

Therefore this analysis shows that the SAT landscape of the problem, namely the zero temperature liquid phase, is composed by two phases: for small $p_0 < p_0^G$ we get a unique ergodic component. Crossing p_0^G one gets a spin glass phase [26] similar to the Gardner phase of amorphous solids [32, 33] in which the ergodicity of the liquid phase breaks down. Indeed the transition point is a continuous replica symmetry breaking transition. In the $g(q) = q^2/2$ case we have the additional spin inversion symmetry which does not typically pertain to the Gardner phase, see the discussion in [34]. However we expect that the properties of the landscape will stay qualitative unchanged for $g(q) = q^2/2 + \epsilon q$ for $\epsilon \ll 1$ which does not have a spin inversion symmetry and which we expect by continuity argument that has a continuous RSB transition, this time of the same nature of the Gardner phase. Therefore the first result that we get is that the model has a Gardner transition that separates the zero temperature liquid phase into two regions. We note that in [35] an analysis of the landscape of Voronoi models, as compared to the Gardner phase found in amorphous solids, was performed providing evidences of a hierarchical landscape structure of local minima in the solid phase beyond the rigidity point. Here we emphasize that the Gardner/RSB transition happens *before* the rigidity transition is crossed, within the liquid phase. Anyway, as we will see, the rigid/solid phase is in a Gardner/RSB phase too and therefore our model provides a theoretical understanding for the numerical findings in [35].

In order to enter the Gardner phase we need to solve the RSB equations. Here we will provide a detailed derivation of the solution.

The first step towards the RSB solution is to consider the PDEs in Eqs. (13) and (14). We will show that they can be easily solved. We start by Eq. (13). In the zero temperature limit, in the SAT phase we expect $q_M < 1$ and therefore we get

$$m(q_M, h) = -\frac{h}{g(1) - g(q)} \quad (30)$$

We will now seek for a solution of the corresponding PDE of the form

$$m(q, h) = -\frac{h}{R(q)}. \quad (31)$$

The function $R(q)$ must be determined by plugging this form into the PDE to get

$$\dot{R}(q) = -x(q)\dot{g}(q) \quad (32)$$

which, using Eq. (30), can be solved as

$$R(q) = g(1) - g(q_M) + \int_q^{q_M} dp x(p)\dot{g}(p). \quad (33)$$

We now turn our attention to Eq. (14). The boundary condition of the PDE is

$$P(q_m, h) = \frac{\exp \left[-(h + p_0)^2 / (2g(q_m)) \right]}{\sqrt{2\pi g(q_m)}} \quad (34)$$

which suggests to seek for a solution of the form

$$P(q, h) = \frac{\exp[-(h + S(q))^2/(2D(q))]}{\sqrt{2\pi D(q)}}. \quad (35)$$

Plugging this ansatz into the PDE we get that

$$S(q) = p_0 \frac{R(q)}{R(q_m)} \quad (36)$$

and

$$\begin{cases} \dot{D}(q) = \dot{g}(q) \left[1 - \frac{2x(q)D(q)}{R(q)} \right] \\ D(q_m) = g(q_m). \end{cases} \quad (37)$$

The solution of the differential equation for $D(q)$ can be written as

$$D(q) = \left[\frac{g(q_m)}{R^2(q_m)} + \int_{q_m}^q \frac{dp \dot{g}(p)}{R^2(p)} \right] R^2(q). \quad (38)$$

The final equation for $x(q)$ is given by Eq. (15) which can be written as

$$\frac{q_m}{\lambda^2(q_m)} + \int_{q_m}^q \frac{dp}{\lambda^2(p)} = \alpha \dot{g}(q) \frac{D(q) + S^2(q)}{R^2(q)}. \quad (39)$$

Note that this last equation shows that $q_m = 0$ for $g(q) = q^2/2$ because of spin inversion symmetry. It is convenient to write the solution of the equation using directly Eq. (17). This gives

$$x(q) = \frac{\alpha \lambda(q)}{2} \frac{\ddot{g}(q)(D(q) + S^2(q)) + 4\dot{g}(q)\ddot{g}(q)}{\frac{R^2(q)}{\lambda^2(q)} + \alpha \lambda(q) \frac{(\dot{g}(q))^3}{R(q)}}. \quad (40)$$

In the $g(q) = q^2/2$ case we get

$$x(q) = \frac{2\alpha q \lambda^3(q) R(q)}{R^3(q) - \alpha q^3 \lambda^3(q)}. \quad (41)$$

We can solve the equation for $x(q)$ in a numerical way as described in the appendix. We now report the results of the numerical solution of these equations. We will focus on $\alpha = 1/4$ and $g(q) = q^2/2$. In this case the Gardner transition happens at $p_0^G = 1$. In fig.1 we report the numerical solution for $x(q)$.

We clearly see that increasing p_0 the support of $x(q)$ extends up to $q_M = 1$. In the right panel we report the dependence of q_M as a function of p_0 . We estimate that the SAT/UNSAT transition happens at $p_0 \simeq 1.871$. Furthermore we clearly see that $1 - q_M \propto p_0^* - p_0$.

D. The UNSAT/Solid (glassy) phase

Having found the rigidity or SAT/UNSAT transition coming from the liquid phase, we turn our attention to the solution of the model in the solid/UNSAT phase. In this case we look for a scaling solution of the RSB equations in the $T = 0$ limit. It is easy to see by inspection that the saddle point equations admit the following scaling solution

$$\begin{aligned} q_M &= 1 - \chi T \\ \hat{m}(1, h) &= \lim_{T \rightarrow 0} T m(q_M, h) = -\frac{h}{1 + \chi \dot{g}(1)} \\ y(q) &= \lim_{T \rightarrow 0} \beta x(q). \end{aligned} \quad (42)$$

Plugging this scaling ansatz in the RSB equations we get

$$\begin{cases} \dot{\hat{m}}(q, h) = -\frac{\dot{g}(q)}{2} \left[\frac{\partial^2 \hat{m}(q, h)}{\partial h^2} + 2y(q)\hat{m}(q, h)\hat{m}'(q, h) \right] \\ m(q_M, h) = -\frac{h}{1 + \chi \dot{g}(1)}. \end{cases} \quad (43)$$

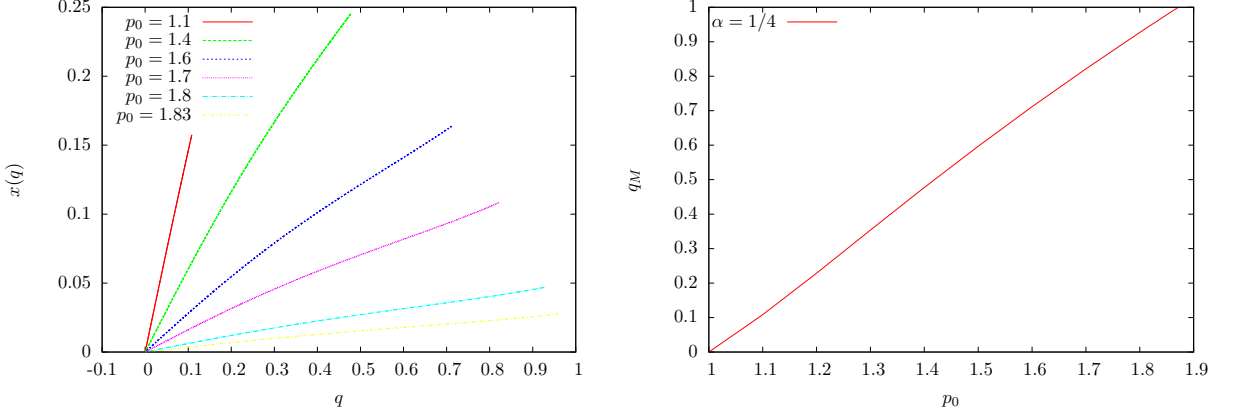


FIG. 1: Left Panel: the solution for $x(q)$ for some values of p_0 in the Gardner phase. The support of this function is in $[0, q_M(p_0)]$. We have realized this plot by solving the RSB equations (see the appendix) for $\alpha = 1/4$ and with $N_{\text{RSB}} = 10000$ steps of replica symmetry breaking. Right Panel: the dependence of q_M as a function of p_0 .

Furthermore the equation for $P(q, h)$ becomes

$$\begin{cases} \dot{P}(q, h) = \frac{\dot{g}(q)}{2} [P''(q, h) - 2y(q)(P(q, h)\hat{m}(q, h))'] \\ P(q_m, h) = \frac{\exp[-(h+p_0)^2/(2g(q_m))]}{\sqrt{2\pi g(q_m)}}. \end{cases} \quad (44)$$

We now proceed as before and solve the equations using a simple ansatz of the same form as in the SAT phase. The equation for \hat{m} can be solved by the following ansatz

$$\hat{m}(q, h) = -\frac{h}{\hat{R}(q)} \quad (45)$$

with

$$\hat{R}(q) = 1 + \chi \dot{g}(1) + \int_q^1 dp \dot{g}(p) y(p). \quad (46)$$

Analogously, for $P(q, h)$ we get

$$\begin{aligned} P(q, h) &= \frac{\exp[-(h + \hat{S}(q))^2/(2\hat{D}(q))]}{\sqrt{2\pi \hat{D}(q)}} \\ \hat{S}(q) &= p_0 \frac{\hat{R}(q)}{\hat{R}(0)} \\ \hat{D}(q) &= \left[\frac{g(0)}{\hat{R}^2(0)} + \int_0^1 \frac{dp \dot{g}(p)}{\hat{R}^2(p)} \right] \hat{R}^2(q). \end{aligned} \quad (47)$$

Finally, the equation that determines χ is

$$\frac{q_m}{\hat{\lambda}^2(q_m)} + \int_{q_m}^1 \frac{dp}{\hat{\lambda}^2(p)} = \alpha \dot{g}(q) \frac{\hat{D}(1) + \hat{S}^2(1)}{\hat{R}^2(1)} \quad (48)$$

where

$$\hat{\lambda}(q) = \beta \lambda(q) = \chi + \int_q^1 dp y(p). \quad (49)$$

The numerical solutions of these equations give the profile of $y(q)$ as well as the value of χ . We will focus again on $g(q) = q^2/2$ and $\alpha = 1/4$ so that $q_m = 0$. In Fig. 2, left panel, we plot the profile of $y(q)$ for some values of p_0 after

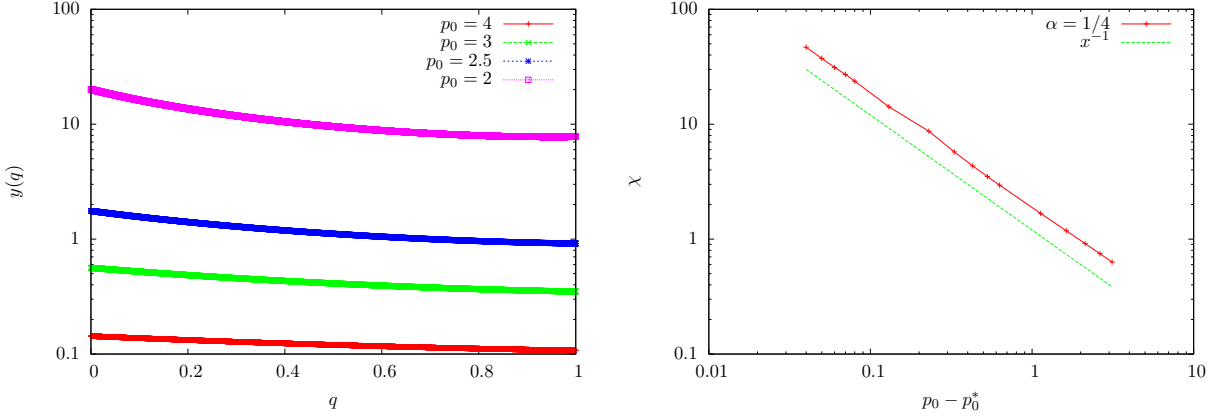


FIG. 2: Left panel: the profile of $y(q)$ for different values of $p_0 > p_0^*$. On approaching the SAT/UNSAT transition $y(q)$ diverges. Right panel: the behavior of χ as a function of the distance from the SAT/UNSAT transition. The green line is $\sim x^{-1}$ and it is shown only as a guide to the eye.

the SAT/UNSAT transition point. We clearly see that $y(q)$ diverges on approaching the unjamming or SAT/UNSAT transition from the UNSAT side. This is consistent with the fact that when we cross the critical point, $x(q)$ must be finite. The same divergence can be found in the behavior of χ which must diverge at the critical point since in the UNSAT phase $q_M < 1$. In the right panel of Fig. 2 we plot the behavior of χ as a function of the distance from the SAT/UNSAT transition (whose value has been estimated by solving the equations on the SAT side and looking at the point where $q_M \rightarrow 1$). We see that $\chi \sim (p_0 - p_0^*)^{-1}$.

E. The effective shape index as a function of the target one

We conclude the analysis by computing the average shape index as a function of the target one. this computation requires to use the solution of the RSB equations in the UNSAT phase. We get

$$\bar{h} = p_0 \left(1 - \frac{1}{\hat{R}(0)} \right) \quad (50)$$

In Fig. (3) we plot the average shape index as obtained from the RSB solution and compare it with numerical simulations. The numerical simulations have been performed with the algorithm described in the appendix which is a form of greedy gradient descent dynamics. Therefore in principle it is not looking for the ground state. Anyway we see that the thermodynamic computation that we have performed compares reasonably well with the numerical simulations. A detailed analysis of out of equilibrium dynamics in the large N limit is certainly possible with dynamical mean field theory and will be presented in a forthcoming work. This will be also important to establish whether the thermodynamic SAT/UNSAT rigidity transition coincides or not with the one of out-of-equilibrium greedy algorithms. In the UNSAT phase a detailed analysis of the landscape of local minima is also possible due to the intrinsic Gaussianity of the model. This will be presented along with the dynamical treatment in a future work.

IV. DISCUSSION AND CONCLUSIONS

We constructed a simple mean field model for the zero temperature rigidity transition in confluent tissues. The model is based on a mapping of the optimization problem of minimizing the cost function of generic Vertex/Voronoi models to a random continuous constraint satisfaction problem with inequality constraints. The liquid phase at zero temperature of tissue models corresponds to the SAT phase of the CCSP. Remarkably we find that the before the SAT/UNSAT transition, corresponding to the rigidity transition in biological tissues, one has a Gardner transition in which the SAT landscape undergoes an ergodicity breaking described by replica symmetry breaking. The transition point shares many similarities with amorphous solids and their Gardner phase. The occurrence of this phase in real models of tissues must be carefully checked in numerical simulations.

We note that at finite temperature, the Gardner point gives rise to a full Gardner transition line, which shares the same properties as a spin glass transition. Note that this is possibly different than the mean field dynamical

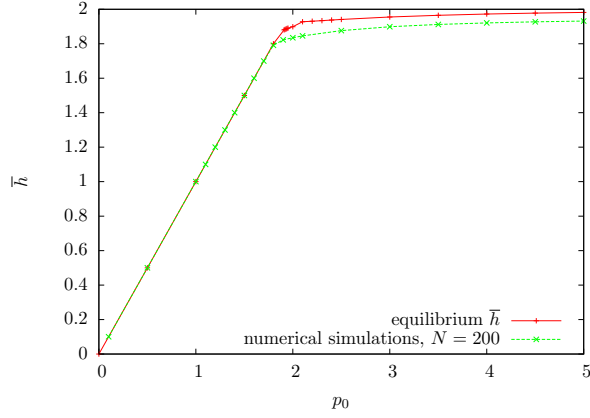


FIG. 3: The shape index as a function of the target one. In green line we have the result of the numerical simulations for $N = 200$ and $\alpha = 1/4$ for the case $g(q) = q^2/2$. In red we have the result of the thermodynamic analysis. In principle the two curves are not the same. However we see that the thermodynamic analysis gives a good approximation both for the SAT/UNSAT transition of greedy algorithms and for the average shape index in the solid phase. Whether the SAT/UNSAT transition of the off-equilibrium data coincides with the thermodynamic one must be carefully investigated both from a dynamical and from a landscape point of view.

glass/mode-coupling transition describing the mean field formation of ergodic glassy components in Random First Order Transition theories [22]. This could provide some explanations for the anomalous glassy dynamics found in [13]. However a careful investigation is mandatory. We underline that the dynamical solution of the model in the large N limit is definitely possible and will be presented elsewhere. This will also allow to include the effects of driving forces such as shear strain and activity. Finally, it would be interesting to develop an analysis of the Hessian of harmonic fluctuation at zero temperature as in [36]. Here the analysis could be carried on by using the technique as developed in [37]. We can foresee that the result of this analysis in the solid phase will give rise to a gapless density of states following $D(\omega) \sim \omega^\nu$ law with $\nu = 2$. This is because the solid phase is marginally stable and therefore the spin glass divergence is divergent by linear fluctuations [41]. This seems different from what observed in [13] where a smaller value of ν seems to be observed (even if the simulations of [13] seem to be not sufficient to conclude for any value of ν). However we note that in $d = 2$ where the simulations of [13] are performed, one expects also the presence of a phononic spectrum which in $2d$ gives rise to $D(\omega) \sim \omega^{1/2}$. This spectrum may hide the modes corresponding to marginal stability of the underlying energy landscape. Therefore it would be important to repeat the numerical simulations of [13] in higher dimensions.

Finally we would like to underline that the class of constraint satisfaction problems introduced in this work is rather interesting. The interest is also due to the fact that, while the UNSAT phase depends on the cost function and the square loss considered in this work represents a rather simple case [42], the SAT phase and the thermodynamic SAT/UNSAT transition is cost-function independent and therefore the analysis presented here is essentially exact. The nature of the solution and RSB of the SAT phase is different from other cases, see [15], where it is much more involved (and richer) due to the emergence of non-linear excitations at the SAT/UNSAT transition point. However the simplicity of the model presented here may be useful to address questions on out-of-equilibrium dynamics which will be the subject of forthcoming works.

Acknowledgments

I would like to thank D. Dumont and C. Nardini for discussion on a related project which motivated this work and D. Dumont for a careful numerical verification of some of the results of [12]. I would like also to thank R. Guida, F. David and V. Ros for useful discussions. This work is supported by 'Investissements d'Avenir' LabEx PALM (ANR-10-LABX-0039-PALM).

Appendix A: Algorithm for the numerical solution of the RSB equations

We will give a detailed account on the numerical procedure to solve the RSB equations. Since this is essentially the same for the SAT and UNSAT phase, we will write explicitly the algorithm only for the SAT phase. We will also

focus on the case $g(q) = q^2/2$. We need to find the profile $x(q)$ and the value of q_M . In a nutshell the algorithm works by starting from a guess of q_M and construct $x(q)$ by integrating backwards the equations for λ and R . From the estimate of $x(q)$ one can recompute a new guess for q_M .

The pseudocode is the following. We discretize the interval $[0, q_M]$ in $L - 1$ 'time' steps and define $dt = q_M/(L - 1)$. Then we go as follows:

1. Start from a guess for $q_M < 1$

2. initialize:

$$\begin{aligned}\lambda(q_M) &= 1 - q_M \\ R(q_M) &= g(1) - g(q_M) \\ x(q_M) &= \frac{2\alpha q_M \lambda^3(q_M) R(q_M)}{R^3(q_M) - \alpha q_M^3 \lambda^3(q_M)}\end{aligned}\tag{A1}$$

3. for $i = 1$, to $i = L - 1$ do

- (a) get $\lambda(q_i)$ from Eq. (18)
- (b) get $R(q_i)$ from Eq. (33)
- (c) get $x(q_i)$ from Eq. (40)

4. update q_M by

$$\begin{aligned}q_M^{\text{new}} &= \alpha \dot{q}(q_M) \frac{D(q_M) + S^2(q_M)}{R^2(q_M)} - \int_0^{q_M} \frac{dp}{\lambda^2(p)} + q_M \\ q_M &\leftarrow \tau q_M^{\text{new}} + (1 - \tau)q_M\end{aligned}\tag{A2}$$

5. repeat points 3 and 4 up to convergence

Note that we have introduce a damping factor τ to remove dangerous oscillations that could disturb the convergence to the fixed point.

Appendix B: Numerical simulations

Numerical minimizations were performed to produce the data plotted in Fig.3. Here we outline the numerical algorithm. We followed the very same strategy as in [36] which we recall here. We used the `bfgs2` routine of the `GSL` library [38]. However since there is a spherical constraint we cannot use the routine as it is implemented. We overcome the problem by define a new Hamiltonian

$$\hat{H}(\underline{x}) = H\left(\frac{\sqrt{N}\underline{x}}{|\underline{x}|}\right) + \frac{A}{4}(|\underline{x}|^2 - N)^2\tag{B1}$$

The first term of \hat{H} is automatically computed on a vector whose with the right length. The second term instead fixes the norm of the vector \underline{x} to the desired value. The constant A can be chosen to be of order one.

Appendix C: A comment on infinite dimensional models

We wanted just to point out that while the model presented in this paper is rather simple and schematic, one could develop a first principle theory in the large dimensional limit. In order to clarify this point we consider a set of N points in d dimensions. We focus now on Voronoi models. For a given point x_i (now a vector in d dimension) the d -dimensional volume of the corresponding Voronoi cell can be written as

$$\mathcal{V}_i(\underline{x}) = \int dy \prod_{j \neq i} \theta(|x_j - y| - |x_i - y|)\tag{C1}$$

It is useful to defined a modified volume as

$$\mathcal{V}_i(\underline{x}, \sigma) = \int dy \prod_{j \neq i} \theta(|x_j - y| - |x_i - y| + \sigma). \quad (\text{C2})$$

The surface of the corresponding Voronoi cell can be obtained as

$$\mathcal{S}_i(\underline{x}) = \left. \frac{\partial \mathcal{V}_i(\underline{x}, \sigma)}{\partial \sigma} \right|_{\sigma=0} \quad (\text{C3})$$

We note that in infinite dimensions $d \rightarrow \infty$, we expect that $V_i \sim e^{d\Sigma}$ and the surface has the same scaling as well. Therefore one can define the shape index as

$$s_i(\underline{x}) = \frac{\mathcal{S}_i(\underline{x})}{\mathcal{V}_i(\underline{x}, 0)} = \left. \frac{\partial}{\partial \sigma} \ln \mathcal{V}_i(\underline{x}, \sigma) \right|_{\sigma=0} \sim d \quad (\text{C4})$$

and consider an Hamiltonian of the form

$$H(\underline{x}) = \frac{1}{2d^2} \sum_i^N (s_i(\underline{x}) - s_0)^2. \quad (\text{C5})$$

The interesting interpretation that comes out from this formulation is that, as it is evident from Eq. (C4), the shape index $s_i(\underline{x})$ is a response function computed as the derivative of a local free energy. This is also true in the mean field model as it is evident from the definition of the impurity problem and the expression of the average shape index.

[1] S. Sinha, A. N. Malmi-Kakkada, X. Li, H. S. Samanta, and D. Thirumalai, *Soft Matter* **16**, 5294 (2020).

[2] S. Sinha and D. Thirumalai, *The Journal of Chemical Physics* **153**, 201101 (2020).

[3] E. R. Kandel, J. H. Schwartz, T. M. Jessell, S. Siegelbaum, A. J. Hudspeth, S. Mack, et al., *Principles of neural science*, vol. 4 (McGraw-hill New York, 2000).

[4] D. C. Van Essen, *Proceedings of the National Academy of Sciences* **117**, 32868 (2020).

[5] T. Tallinen, J. Y. Chung, F. Rousseau, N. Girard, J. Lefèvre, and L. Mahadevan, *Nature Physics* **12**, 588 (2016).

[6] D. Bi, X. Yang, M. C. Marchetti, and M. L. Manning, *Physical Review X* **6**, 021011 (2016).

[7] D. Bi, J. Lopez, J. M. Schwarz, and M. L. Manning, *Nature Physics* **11**, 1074 (2015).

[8] L. Yan and D. Bi, *Physical Review X* **9**, 011029 (2019).

[9] D. M. Sussman and M. Merkel, *Soft matter* **14**, 3397 (2018).

[10] M. Merkel and M. L. Manning, *New Journal of Physics* **20**, 022002 (2018).

[11] M. Merkel, K. Baumgarten, B. P. Tighe, and M. L. Manning, *Proceedings of the National Academy of Sciences* **116**, 6560 (2019).

[12] O. K. Damavandi, V. F. Hagh, C. D. Santangelo, and M. L. Manning, *Physical Review E* **105**, 025004 (2022).

[13] D. M. Sussman, M. Paoluzzi, M. C. Marchetti, and M. L. Manning, *EPL (Europhysics Letters)* **121**, 36001 (2018).

[14] S. Franz and G. Parisi, *Journal of Physics A: Mathematical and Theoretical* **49**, 145001 (2016).

[15] S. Franz, G. Parisi, M. Sevelev, P. Urbani, and F. Zamponi, *SciPost Physics* **2**, 019 (2017).

[16] C. Brito, H. Ikeda, P. Urbani, M. Wyart, and F. Zamponi, *Proceedings of the National Academy of Sciences* **115**, 11736 (2018).

[17] H. Ikeda, P. Urbani, and F. Zamponi, *Journal of Physics A: Mathematical and Theoretical* **52**, 344001 (2019).

[18] S. Franz, A. Sclocchi, and P. Urbani, *Physical review letters* **123**, 115702 (2019).

[19] A. Sclocchi and P. Urbani, *SciPost Phys.* **10**, 13 (2021), URL <https://scipost.org/10.21468/SciPostPhys.10.1.013>.

[20] A. Sclocchi and P. Urbani, *Physical Review E* **105**, 024134 (2022).

[21] P. Charbonneau, J. Kurchan, G. Parisi, P. Urbani, and F. Zamponi, *Nature communications* **5**, 1 (2014).

[22] G. Parisi, P. Urbani, and F. Zamponi, *Theory of simple glasses: exact solutions in infinite dimensions* (Cambridge University Press, 2020).

[23] P. Charbonneau, E. I. Corwin, R. C. Dennis, R. D. H. Rojas, H. Ikeda, G. Parisi, and F. Ricci-Tersenghi, *Physical Review E* **104**, 014102 (2021).

[24] S. Franz, A. Sclocchi, and P. Urbani, *SciPost Physics* **9**, 012 (2020).

[25] Y. V. Fyodorov, *Journal of Statistical Physics* **175**, 789 (2019).

[26] M. Mezard, G. Parisi, and M. A. Virasoro, *Spin glass theory and beyond* (World Scientific, Singapore, 1987).

[27] M. Mézard and G. Parisi, *Journal de Physique I* **1**, 809 (1991).

[28] G. Parisi, *Journal of Physics A: Mathematical and General* **13**, L115 (1980).

[29] H.-J. Sommers and W. Dupont, *Journal of Physics C: Solid State Physics* **17**, 5785 (1984).

- [30] J. R. de Almeida and D. J. Thouless, *Journal of Physics A: Mathematical and General* **11**, 983 (1978).
- [31] H.-J. Sommers, *Journal de Physique Lettres* **46**, 779 (1985).
- [32] J. Kurchan, G. Parisi, P. Urbani, and F. Zamponi, *J. Phys. Chem. B* **117**, 12979 (2013), URL <https://pubs.acs.org/doi/10.1021/jp402235d>.
- [33] P. Charbonneau, J. Kurchan, G. Parisi, P. Urbani, and F. Zamponi, *Annual Review of Condensed Matter Physics* **8**, 265 (2017).
- [34] P. Urbani and G. Biroli, *Phys. Rev. B* **91**, 100202 (2015).
- [35] D. E. Pinto, D. M. Sussman, M. M. T. da Gama, and N. A. Araújo, *Physical Review Research* **4**, 023187 (2022).
- [36] S. Franz, G. Parisi, P. Urbani, and F. Zamponi, *Proc. Natl. Acad. Sci. U.S.A.* **112**, 14539 (2015).
- [37] P. Urbani, arXiv preprint arXiv:2203.01899 (2022).
- [38] M. e. a. Galassi, *GNU Scientific Library Reference Manual* (3rd Ed.).
- [39] A convex tessellation is made out of cells that are convex polygons.
- [40] This is the number of vertices or points in Vertex and Voronoi models respectively, multiplied by the dimensionality of the system.
- [41] Note that for the model presented in this model marginal stability is realized at the level of linear excitations.
- [42] We note that introducing higher than quadratic term in the cost function gives rise also to non-linear excitations which may affect the way in which marginal stability is realized